α-Helix Structure in Alzheimer's Disease Aggregates of Tau-Protein†

Mourad Sadqi,‡ Felix Hernández,§ UnMei Pan,‡ Mar Pérez,§ Michael D. Schaeberle,|| Jesús Ávila,§ and Victor Muñoz*,‡

Department of Chemistry and Biochemistry and Center for Biomolecular Structure and Organization, University of Maryland, College Park, Maryland 20742, Centro de Biología Molecular Severo Ochoa, Universidad Autónoma de Madrid, 28049 Madrid, Spain, and Laboratory of Chemical Physics, National Institute of Diabetes and Digestive and Kidney Diseases, National Institutes of Health, Bethesda, Maryland 20892

Received March 6, 2002; Revised Manuscript Received April 5, 2002

ABSTRACT: The discovery of β-sheet structure in Alzheimer's amyloid fibrils, and then in many other disease-related protein fibrils, has led to the widely believed view that β-sheet formation is the general mechanism of aberrant protein aggregation leading to disease. This notion is further reinforced by recent findings, which indicate that normal proteins can be induced to form β-sheet fibrils in vitro. Alzheimer's disease, a paradigm proteopathy, is accompanied by the formation of two distinct aggregates, amyloid fibrils and paired helical filaments (PHFs). Electron microscope images of PHFs show pairs of twisted ribbons with 80 nm periodicity. However, there is little information of the molecular structure of PHFs, as previous studies have failed to identify signs of regular structure. Using far-UV circular dichroism and Fourier-transformed infrared spectroscopy, we find that PHFs are comprised of α-helices. This is remarkable as tau-protein, PHF's primary constituent, has a high abundance of helix-breaking amino acids and is unstructured in solution. We also find that PHFs are very stable, as judged by their high melting temperature and resistance to protease digestion. PHFs are the first example of pathological aggregation associated to the formation of α-helix.

Aberrant aggregation of proteins is critical to the onset of many human diseases (*1*). The discovery of β-sheet structure, first in Alzheimer's disease (AD) amyloids (*2*, *3*) and then in fibrils related to many other diseases (*4*), has led to the widely held idea that aberrant protein aggregation must involve formation of intermolecular β-sheets. This concept has been further reinforced by recent findings indicating that normal proteins can also be induced to form β-sheet fibrils in vitro (*5*, *6*). In contrast with amyloids, very little is known about the structure of paired helical filaments (PHFs), the other protein aggregates related to AD. PHFs were named for their appearance under the electron microscope as a pair of ribbons twisted around each other (*7*, *8*). The ultrastructure of PHFs has been intensively investigated by electron microscopy and atomic force microscopy (*7*−*11*). These studies show a helical pitch of typically ∼80 nm with widths of 10 and 22 nm in the narrow and wide points, respectively. Previous X-ray fiber diffraction analysis of poorly aligned samples of tangled PHFs have failed to show signs of regular structure (*12*). The observation by Fourier-transformed infrared spectroscopy (FTIR) of an amide I maximum at 1658 cm^{-1} was interpreted as additional evidence of the lack of ordered structure in PHFs (*12*). Recent structural studies of fibers grown in vitro from diverse recombinant tau-constructs are even more perplexing. The molecular structure and structural homogeneity of these in vitro grown fibers vary widely depending on polymerization conditions and the tau-constructs used in the assay (*13*, *14*). The goal of this paper is to investigate in more detail the molecular structure of bona fide PHFs. To achieve this, we use a combination of FTIR and far-UV circular dichroism (CD) spectroscopy.

MATERIALS AND METHODS

Isolation and Handling of PHFs and Tau(3 + 2). PHFs were isolated from brain samples of AD patients following the standard procedure of Greenberg and Davies (*15*). Brain tissue was supplied by Dr. Ravid (Netherlands Brain Bank). Recombinant tau(3 + 2) (the longest three repeat isoform) has been obtained as previously described (*16*).

Electron Microscopy. Negative-staining electron microscopy was performed in a JEOL model 1200EX electron microscope operated at 100 kV.

Immunoblotting and Immunoelectron Microscopy. Immunoblotting and immunoelectron microscopy were carried out as described previously (*16*).

Determination of PHFs Concentration and Purity. Peptide bond concentration in PHFs samples was determined by measuring the absorbance of the peptide bond band at 192 nm. Two different molar extinction coefficients have been used in this determination: a ϵ_{192} of 7960 cm^{-1} M^{-1} per peptide bond, which was obtained experimentally from horse heart cytochrome *c* (105 amino acids) comparing its absorption at 192 and 410 nm (Soret band, ϵ_{410} = 110 000 cm^{-1}

† V.M. is the recipient of a Dreyfus New Faculty Award, a Packard Fellowship, and a Searle Scholarship.

* To whom correspondence should be addressed. Department of Chemistry and Biochemistry, University of Maryland, College Park, MD 20742. Tel.: 1-301-405-3165. Fax: 1-301-314-0386. E-mail: vm48@umail.umd.edu.

‡ University of Maryland.

§ Universidad Autónoma de Madrid.

|| National Institutes of Health.

10.1021/bi025777e CCC: $22.00
Published on Web 05/07/2002

M^{-1}), and a ϵ_{192} of 7110 cm^{-1} M^{-1} per peptide bond. The latter was obtained from the direct comparison between the absorbance values at 192 and 280 nm (i.e., $\epsilon_{280} = 5690$ cm^{-1} M^{-1} for Trp (*17*)) in a series of peptides with template sequence (Ala-Gly-Gln)*n*-Trp and *n* ranging from 1 to 5. These two molar extinction coefficients probably constitute upper and lower limits, respectively, of the mean residue molar extinction coefficient of tau in PHFs. While tau has a smaller proportion of aromatic residues than horse heart cytochrome *c*, it has a large content of side chains with significant absorbance in the 192 nm region (e.g., His, Arg, Glu, Lys, and Asp (*18*)). Purity of PHFs preparations was also determined spectroscopically by comparing the absorbance values at 192 (peptide bond) and 220 nm ($\epsilon_{220} =$ 35 000 for Trp). This can be done because proteins average 1 Trp residue per 100 amino acids, while tau-isoforms (with more than 400 residues) completely lack tryptophan and, therefore, have an absorption spectrum with no signs of a shoulder at 220 nm (data not shown).

FTIR Spectroscopy. The infrared absorption spectra of PHFs and myoglobin were collected on samples dried on a glass slide using an infrared spectrometer (Bruker, IFS 66/s) coupled to an IR microscope (Bruker, IR Scope II) equipped with a mercury−cadmium−telluride single-point detector at the end of the optical train. One hundred coadded scans were collected over the 400−3950 cm^{-1} spectral range at 4 cm^{-1} resolution. The resulting interferogram was fast Fourier-transformed using Mertz apodization.

PHF Sonication Experiments. Sonication of PHFs was performed in a solution of PHFs at 0.5 mg/mL using a B. Braun, model Labosonic 2000U, at the maximum power in cycles of 15 s for a total of 2 min. The CD spectrum of the PHF sample was recorded after every sonication cycle. Sonication breaks PHFs in clean fractures by shear forces resulting from cavitation. Because the shear field is proportional to the length of the polymer, sonication is expected to progressively reduce the length of PHFs up to a critical size.

Far-UV CD. All far-UV CD spectra were obtained with an Applied Photophysics 180 PiStar instrument. Standard measurements were carried out at 25 °C in very dilute PHF solutions (20 mM phosphate buffer at pH 7) on a cylindrical 0.1 cm path length cuvette. CD spectra were recorded from 250 to 190 nm every 1 nm by averaging 2 million 250 μs measurements (500 s total integration time per point). Experimental uncertainty was determined at each wavelength from the standard deviation of the 2 million measurements. No baseline drifts were observed during the collection time of a complete spectrum. Thermal denaturation experiments were carried out using a computer-controlled Neslab RE-111 and a thermostated cuvette holder. Real cuvette temperatures were measured with a thermocouple. Thermal denaturation curves were done increasing PHF concentration by a factor of 3 and decreasing the acquisition time by a factor of 10 (i.e., 25 μs per measurement) to reduce the total collection time of the experiment.

Fitting of CD Data. Secondary structure content in PHFs was obtained by least-squares fitting to linear combinations of the three basis CD spectra (*19*). We calculated the sum of least squares for each possible linear combination and the experimental CD spectrum multiplied by a scaling factor to account for possible errors in the concentration determination. The set of solutions compatible with the experimental uncertainty in the CD signal was identified as all linear combinations with sums of least squares less than 60% higher than the minimal. The statistically most likely secondary structure content of PHFs is calculated as the average of all experimentally compatible solutions weighted by a simple function of the scaling factor and of the difference in the sum of least squares with the best fit, i.e., $w = 1/((SLS - SLS_{min})(1 + |1 - sf|))$. This procedure has been carried out in CD spectra corrected for protein concentration using both molar extinction coefficients (see above). The global results of this procedure render an α-helix content of (85 ± 9)%, a β-sheet content of (4 ± 3)%, and a random coil content of (11 ± 5)%. For all compatible solutions, the scaling factor was larger than 1, indicating an overestimation of the peptide bond concentration in PHFs of ∼12 to ∼22% depending on the molar extinction coefficient. This error may be due to the presence of counterions tightly bound to the many charged residues of tau-protein. The same procedure was applied to the fitting of the CD data to basis spectra of α-helices of varying length (*19*). In this case, the best fit was obtained for an α-helix of 11 residues, and the weighted average was 13 ± 8 residues.

Singular Value Decomposition (SVD) of CD Data. SVD of the matrix of CD spectra at different temperatures has been performed using the program MATLAB. The result of the SVD was then processed using the rotation and mixing procedures described by Henry and Hofrichter to optimize the autocorrelations for the amplitude matrix (*V*) (*20*). For simplicity, in Figure 4B, the two components have been corrected by a scaling factor to show absolute <residue> ellipticity units. The corresponding inverse correction has been applied to the amplitude vectors. To recover the original values produced by the SVD, the α-helix component must be multiplied by 3.215 and the random coil component by 0.964.

Pronase Digestion Assay. Pronase digestion assays were performed using the protocol described by Wischik et al. (*21*). We incubated ∼1.7 peptide bond μmol of cytochrome *c* or ∼30 peptide bond nmol of PHFs with 75 mU (4 units per mg) of pronase in digestion buffer (1 mM $CaCl_2$, 3 mM $MgCl_2$, and 10 mM phosphate buffer pH 7.0) at 35 °C. Protein digestion was monitored in real time by absorbance and far-UV CD.

RESULTS AND DISCUSSION

Electron microscopy of our PHF samples shows all of the classic ultrastructural characteristics of PHFs (Figure 1A). In these preparations, PHFs have an average length of ∼530 nm with a dispersion of ±235 nm. Immunolabeling with PHF-1 antibody reveals that the polymeric structures observed in Figure 1A are, indeed, bona fide PHFs composed by tau-protein (Figure 1B). The densitometric analysis of silver-stained sodium dodecyl sulfate polyacrylamide gel electrophoresis (SDS−PAGE) gels (Figure 1A, inset) and Western blots (Figure 1B, inset) of our PHF samples indicate that at least 85% of the protein present corresponds to tau-products (*22*). The purity level of our preparations has been further confirmed by absorption spectroscopy (see Materials and Methods).

FTIR is extensively used to investigate the structural properties of protein aggregates. The analysis of the amide

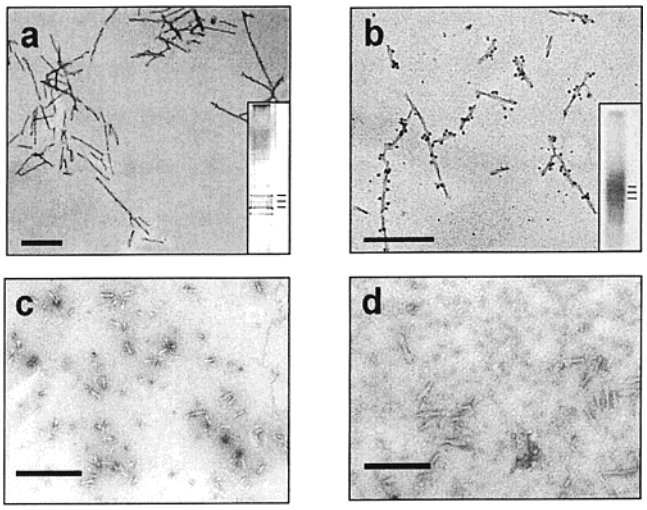

FIGURE 1: Electron microscopy of PHFs. (a) Untreated PHF samples stained with 2% uranyl acetate; (inset) silver-stained SDS−PAGE of PHFs showing the typical tau-bands at 60, 64, and 68 kD. (b) Immunoelectron microscopy of untreated PHFs with PHF-1 antibody; (inset) PHF-1 antibody Western blot analysis of PHFs. (c) PHFs after 2 min of sonication. (d) PHFs after 5 min at 95 °C. Scale bars represent 500 nm.

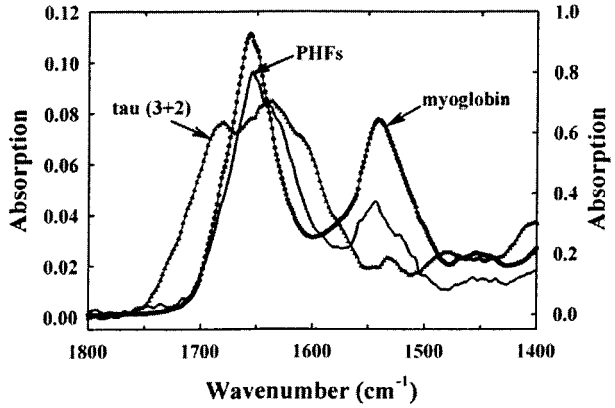

FIGURE 2: Fourier-transformed infrared spectrum of PHFs (continuous line, left absorbance scale), recombinant tau(2 + 3) (triangles, left absorbance scale), and myoglobin (circles, right absorbance scale).

I band frequency provides information on protein secondary structure (*23*, *24*). The amide region of the FTIR spectrum of PHFs is shown in Figure 2. The FTIR spectra of myoglobin, a protein with ∼87% α-helical content as determined by X-ray crystallography, and of full length recombinant tau, i.e., tau(2 + 3), are also included as reference. The absorption maximum for the amide I band of PHFs is observed at 1654 cm^{-1}, in agreement with a previous FTIR study (*12*). This maximum is right in the middle of the range of frequencies typically observed in α-helical structures (*24*). Indeed, it coincides with the observed absorption maximum of myoglobin (i.e., 1656 cm^{-1}). In contrast, tau(2 + 3) has a much broader amide I band, in which several maxima are observed. This reflects the existence of large conformational diversity, as expected in an unstructured protein such as soluble tau (*12*). Deconvolution of the FTIR spectrum of PHFs reveals an additional less-pronounced band at 1642 cm^{-1}, which could be ascribed to a small fraction of disordered structure (*23*). These results suggest that the α-helix is the main component of the molecular structure of PHFs. However, this interpretation is not unique, because there are known examples of nonhelical protein conformations with amide I bands in the same range of frequencies (*24*).

CD is more sensitive to protein secondary structure, especially to the α-helix, than FTIR (*25*). However, its application to protein aggregates is more difficult due to potential optical artifacts from light scattering, birefringence, and linear dichroism (*26*). Moreover, the interpretation of CD data typically requires a precise determination of peptide bond concentration (*26*, *27*). Because PHFs' composition is heterogeneous, i.e., six different tau-isoforms with molecular masses ranging from 40 to 45 kD (*28*), in our CD experiments, we have determined peptide bond concentration directly from the absorption maximum at 192 nm (see Materials and Methods). Light scattering was minimized by performing all of our measurements in very diluted solutions, i.e., 50−300 μM peptide bond corresponding to ∼175−750 nM protein. To assess whether birefringence and linear dichroism were contributing to our recorded CD signal, we sonicated the PHFs. Sonication should decrease any degree of alignment that could be present in the sample by shortening PHFs. Figure 1C shows a PHF sample after 2 min of sonication. It reveals that PHFs are still present and maintain the same ultrastructural properties but are much shorter and more uniform in length (80 ± 18 nm). The CD spectrum of PHFs was totally invariant during the course of an experiment in which the samples were sonicated for a total of 5 min in intervals of 30 s (data not shown), indicating that there is not significant contribution from birefringence or linear dichroism. Therefore, the recorded CD spectrum corresponds to the average peptide bond conformation of tau-protein embedded in the PHF polymer.

The CD spectrum of PHFs is shown in Figure 3A. This spectrum has all of the features of an α-helix. The two deep minima at 222 and 208 nm and the more intense maximum at 193 nm (*26*, *27*) are evident. Simple methods for estimating α-helix content based on the quantitative analysis of the intensity of the CD signal at 222 nm (*29*) indicate that our PHFs samples are ∼70% α-helical. However, these calculations are extremely sensitive to errors in the determination of protein concentration and do not consider end effects in the α-helical CD spectrum. This is of particular relevance in this case, where peptide bond concentration has been determined directly from the absorbance at 192 nm (see Materials and Methods). In an alternative procedure, the α-helix content can be estimated from the ratio between the intensity at 193 and 222 nm (R1 parameter) (*30*). A 12 residue long α-helix (average helix length in proteins (*19*)) has an R1 parameter of −2.57. The R1 parameter is a good indicator of α-helix content because it increases linearly as helix content decreases (*31*). Moreover, it is entirely based on spectral shape and, therefore, unaffected by errors in the determination of protein concentration. For the CD spectrum of our PHF samples, we obtain a R1 parameter of −2.47, which indicates ∼95% of α-helix. The helix content estimated with this method is very large because the shape of the CD spectrum of PHFs is almost identical to that of the α-helix basis CD spectrum (Figure 3B). This comparison highlights the high helical content of PHFs. A more sophisticated calculation involves fitting the experimental CD spectrum to a linear combination of the three basis spectra, i.e., α-helix, β-sheet, and random coil (*19*). An advantage

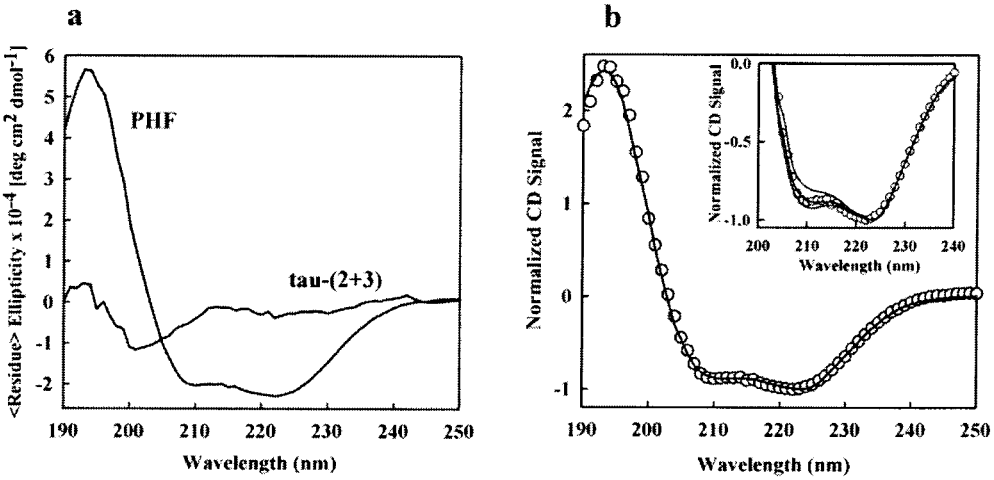

FIGURE 3: Far-UV CD of PHFs. (a) CD spectra of tau(3 + 2) and untreated PHFs at 25 °C. (b) Comparison between the normalized CD spectrum of PHFs (empty circles) and the CD spectrum of a 11 residue long perfect α-helix (line); (inset) detail of the 208−222 nm region of the CD spectrum illustrating CD end effects: PHFs (empty circles), model of an 11 residue α-helix (middle line), model of an 18 residue α-helix (lower line), model of a 7 residue α-helix (upper line); note that in the range of 190−200 nm the agreement between the CD spectrum of PHFs and the model spectrum for a 7 residue α-helix is better than for that of an 18 residue α-helix.

of this procedure is that it allows a statistical evaluation of how the experimental uncertainty, i.e., noise in the CD spectrum and errors in the determination of protein concentration, affects the estimation of secondary structure contents (see Materials and Methods). The results of this analysis indicate that PHFs have an α-helix content of (85 ± 9)%, a content of unstructured coil of (11 ± 5)%, and negligible amounts of β-sheet (4 ± 3)%.

The combination of CD and FTIR shows that the structure of tau-protein in PHFs has a very high proportion of α-helices. The same results have been obtained analyzing PHF samples purified from brain tissue of three different patients. This indicates that the α-helix is an intrinsic property of the structure of PHFs. Importantly, monomeric full-length tau is totally unstructured in solution, as it was found previously by small-angle X-ray scattering (*12*) and here by FTIR and CD (Figures 2 and 3A). The α-helical conformation observed in PHFs is, therefore, entirely induced by intermolecular interactions.

To obtain information on the characteristic length of the α-helices in PHFs, we have taken advantage of the end effects on the CD spectrum of α-helices (*19*, *26*). Fitting the CD spectrum of PHFs to a empirically derived set of basis CD spectra for helices of varying length (*19*) shows that the average helical length in PHFs is ∼13 ± 8 residues (inset, Figure 2B, Materials and Methods). This is strikingly similar to α-helices found in globular proteins (*19*). Therefore, the α-helix structure of PHFs does not arise from long α-helices spanning the complete sequence of tau and arranged in coiled coils, as it has been predicted for cytoskeletal intermediate filaments (*32*). Rather, the molecular structure of PHFs is comprised of arrays of ∼2−6 turns of α-helix connected by short loops.

The question of whether significant segments of protein, e.g., loops, are extruding from the PHF core can be indirectly investigated with protease susceptibility assays. We have used the nonsequence specific protease pronase (*21*) and cytochrome *c* as a control for protease activity. The reaction has been monitored using absorption and CD spectroscopy. Both techniques measure the amount of nondigested protein by detecting peptide bond integrity. In contrast to previous

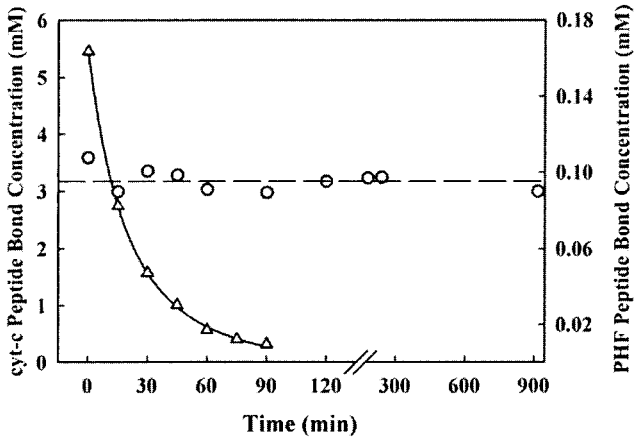

FIGURE 4: Pronase digestion assay; (triangles) cytochrome *c*, (circles) PHFs. The units are in millimoles of peptide bonds per liter. The discontinuous line is a horizontal line to highlight PHFs resistance to pronase digestion. The continuous line is an exponential fit to cytochrome *c* digestion data.

studies of protease susceptibility in PHFs (*21*, *33*), these experiments have been done in mild conditions. The goal is to ensure that only directly accessible protein regions are susceptible to protease attack. In such conditions, total digestion of native cytochrome *c* occurred in less than 90 min. However, under the same conditions, a much smaller initial amount of PHFs was totally unaffected by pronase, even after 24 h of incubation (Figure 4). These results suggest a homogeneous and rigid PHF structure in which both α-helices and loops are tightly embedded in the polymer.

In temperature denaturation experiments of PHFs (Figure 5A), the α-helix structure only starts to melt at ∼74 °C. At the final temperature (88 °C), ∼30% of the initial α-helix content still remains, showing the high thermal stability of PHFs. The melting transition is totally irreversible, as no α-helix CD signal is recovered after cooling the sample back down to 11 °C. This suggests that α-helix unwinding is due to polymer melting and not to partial unfolding of a PHFs' outer layer. Such interpretation is confirmed by electron microscopy of heated PHF samples (Figure 1D), which shows much shorter PHFs (130 ± 18 nm). In fact, there is

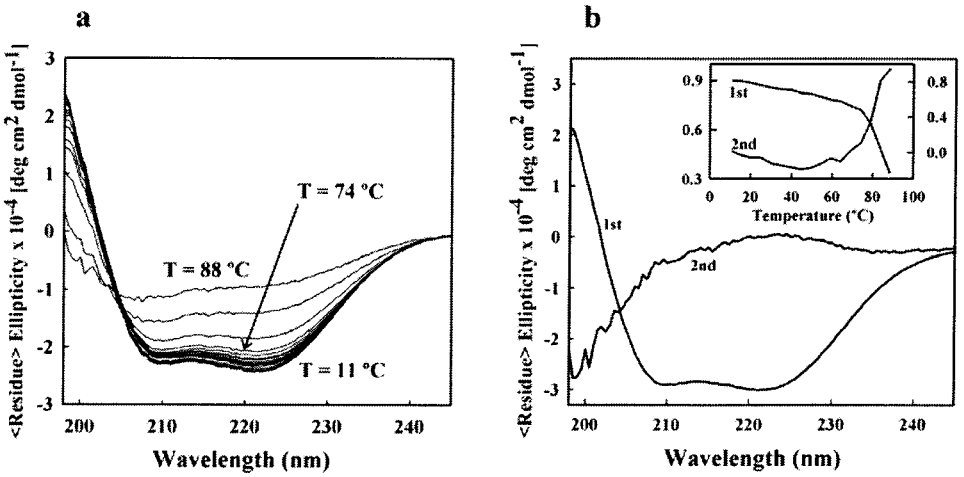

FIGURE 5: Thermal denaturation of PHFs. (a) Series of CD spectra of PHFs at different temperatures (from ~10 to ~89 °C in 5 °C steps). Labels indicate the initial and final temperatures and the temperature of the beginning of PHFs' melting transition. (b) SVD of the thermal denaturation experiment. The main figure shows the first, i.e., α-helix, and second, i.e., random coil, components. The inset shows the amplitude of the α-helix component (left scale) and the amplitude of the random coil component (right scale).

semiquantitative agreement between both observations. Because the average length of heated PHFs, i.e., ~25% of the length before heating, is what is expected if the observed change in CD signal arises from dissociation of tau-molecules from the PHF ends. These observations also argue in favor of a homogeneous PHF structure, instead of a model in which a hard core is coated by fuzzier material.

The SVD of the series of temperature-dependent CD spectra provides further insight into the structural properties of PHFs. On the basis of in vitro polymerization assays of short tau-peptides, it has recently been argued that the core of PHFs might be arranged in an amyloid-like β-sheet conformation (*34*). If this was the case, the thermal denaturation of PHFs should be complex, reflecting the nonconcerted melting of the outer layer and core of PHFs. However, the SVD analysis of the thermal denaturation of PHFs resolves only two components. The first one corresponds to the α-helix, and the second component is a typical random coil CD spectrum (Figure 4B). The amplitude analysis shows a simple two state transition, i.e., no intermediate structures present, in which the α-helix content decreases concomitantly to an increase in the amount of random coil conformations (inset, Figure 5B). The random coil component most likely corresponds to tau-molecules dissociated from PHFs. Therefore, no signs of other kinds of structure, such as β-sheets, are found in the melting of PHFs, which unfolds as a homogeneous structure.

Our experiments show unambiguously that PHFs isolated from AD patients are comprised of α-helix segments of less than ~20 residues connected by short loops. Furthermore, the molecular structure of PHFs is homogeneous, with both the α-helices and the loops embedded in the PHF scaffold. How does this description compare with results obtained from fibers grown in vitro from tau-constructs? Finding an efficient method to produce PHFs in vitro is of great importance to dissect the mechanism of PHF formation. One problem to achieve this goal is the potential lack of specificity of the polymerization assays. This is a critical issue, as it has now become obvious that even normal proteins aggregate in vitro into β-sheet containing fibrils (*6*, *35*−*37*). Another problem is to achieve homogeneity in the self-assembly reaction. Recent X-ray fiber diffraction and FTIR studies of fibers grown from short tau-fragments indicate that it is straightforward to obtain rather homogeneous fibers (*14*). However, all of these fibers are nonspecific, showing the typical pattern of β-sheet structure observed in many other in vitro aggregates (*13*, *14*). Fibers grown from longer tau-constructs are also nonspecific and, furthermore, much less homogeneous (*14*). A recent report of an X-ray fiber diffraction pattern that was compatible with α-helices packed transversally to the long axis of fibers grown from full-length tau is a potentially promising exception (*13*). Clearly, more work is needed in this direction. For these efforts, it is important to characterize the structural properties of the in vitro-assembled material, especially because electron microscopy has been found insensitive to differences in the molecular structure of the fibers (*13*). In this regard, the presence of α-helix structure arises as a powerful structural criterion for the formation of PHF-like fibers.

How surprising are our findings on the structure of PHFs? There are known examples of pathological polymers, like hemoglobin fibers in sickle cell disease (*38*), in which the protein polymerizes maintaining its native α-helical structure. Cytoskeletal intermediate filaments are composed by α-helices arranged together as long-coiled coils (*32*). However, PHFs are the first example of aberrant aggregates in which the formation of α-helix structure is associated to the aggregation process. The α-helix in PHFs is only stabilized by intermolecular interactions. In principle, the amino acid sequence of tau is a counter example of a "good" α-helical sequence, including many prolines and glycines. A calculation with the helix−coil algorithm Agadir (*39*) indicates that the energetic cost of making a full α-helix of tau is ~3.0 kcal/mol per residue, e.g., ~1200 kcal/mol for full length tau. However, this simple calculation clearly overestimates the energetic cost of forming the PHF structure. Many of the glycines and prolines are probably located in loop regions. Furthermore, prolines are helix-promoting residues when placed in the first position of the α-helix (*40*), especially if the preceding residue in the sequence, i.e., N-cap position, is a serine or threonine, like it occurs for many of the prolines from the central region of tau. Glycines are also helix-promoting residues when placed in C-cap positions (*41*). It is also important to consider that while β-sheet aggregates

are stabilized by intermolecular hydrogen bonds, helical hydrogen bonds are intrinsically intramolecular. Therefore, formation of a highly stable α-helical polymer, such as PHFs, must involve very strong side chain−side chain interactions. Tau is positively charged and very hydrophilic, so the most likely candidates are ion pairs, perhaps explaining why tau is found hyperphosphorylated in PHFs. Another appealing structural role for the hyperphosphorylation of tau is suggested by recent findings revealing that phosphorylation of serine and threonine greatly enhances their α-helix-promoting effect as N-caps (*42*).

The PHF is the first member of what could be a whole new family of pathological aggregates formed by the intermolecular packing of α-helices. Understanding the forces that drive the formation and stabilization of α-helical PHFs is clearly a fascinating problem for the structural biologist. From the medical standpoint, deciphering the mechanism of PHF formation is critical to comprehend the molecular basis of AD. Furthermore, obtaining a structural model of the PHF structure could be pivotal for undertaking the de novo drug design of inhibitors of tau-aggregation. The work that we present here constitutes a very first step toward reaching those goals.

ACKNOWLEDGMENT

We thank Eva de Alba, William Eaton, and George Lorimer for helpful comments on the manuscript. We are indebted to Ira Levin for the use of his infrared instrumentation.

REFERENCES

1. Sunde, M., and Blake, C. C. (1998) *Q. Rev. Biophys. 31*, 1039.
2. Kirschner, D. A., Abraham, C., and Selkoe, D. J. (1986) *Proc. Natl. Acad. Sci. U.S.A. 83*, 503−507.
3. Serpell, L. C. (2000) *BBA 1502*, 16−30.
4. Sunde, M., Serpell, L. C., Bartlam, M., Fraser, P., Pepys, C., and Blake, C. C. (1997) *J. Mol. Biol. 273*, 729−739.
5. Dobson, C. M. (1999) *Trends Biochem. Sci. 24*, 329−332.
6. Fandrich, M., Fletcher, M. A., and Dobson, C. M. (2001) *Nature 410*, 165−166.
7. Kidd, M. (1963) *Nature 197*, 192−193.
8. Crowther, R. A., and Wischik, C. M. (1985) *EMBO J. 4*, 3661−3665.
9. Ohtsubo, K., Izumiyama, N., Shimada, H., Tachikawa, T., and Nakamura, H. (1990) *Acta Neuropathol. 79*, 480−485.
10. Pollanen, M. S., Markiewicz, P., Bergeron, C., and Goh, M. C. (1994) *Am. J. Pathol. 144*, 869−873.
11. Pollanen, M. S., Markiewicz, P., and Goh, M. C. (1997) *J. Neuropathol. Exp. Neurol. 56*, 79−85.
12. Schweers, O., Schonbrunn-Hanebeck, E., Marx, A., and Mandelkow, E. (1994) *J. Biol. Chem. 269*, 24290−24297.
13. Gianetti, A. M., Lindwall, G., Chau, M.-F., Radeke, M. J., and Feinstein, S. C. (2000) *Protein Sci. 9*, 2427−2435.
14. von Bergen, M., Barghorn, S., Li, L., Marx, A., Biernat, J., Mandelkow, E. M., and Mandelkow, E. (2001) *J. Biol. Chem. 276*, 48165−48174.
15. Greenberg, S. G., and Davies, P. (1990) *Proc. Natl. Acad. Sci. U.S.A. 87*, 5827−5831.
16. Perez, M., Valpuesta, J. M., Medina, M., Montejo de Garcini, E., and Avila, J. (1996) *J. Neurochem. 67*, 1183−1190.
17. Hill, S. C., and Hippel, P. H. v. (1989) *Anal. Biochem. 182*, 319−326.
18. Wetlaufer, D. B. (1962) *Adv. Protein Chem. 12*, 303−390.
19. Chen, Y.-H., Yang, J. T., and Chau, K. H. (1974) *Biochemistry 13*, 3350−3359.
20. Henry, E. R., and Hofrichter, J. (1992) *Methods Enzymol. 210*, 129−192.
21. Wischik, C. M., Novak, M., Thogersen, H. C., Edwards, P. C., Runswick, M. J., Jakes, R., Walker, J. E., Milstein, C., Roth, M., and Klug, A. (1988) *Proc. Natl. Acad. Sci. U.S.A. 85*, 4506−4510.
22. Ksiezak-Reding, H., Morgan, K., and Dickson, D. W. (1994) *Brain Res. 649*, 185−196.
23. Byler, M., and Susi, H. (1986) *Biopolymers 25*, 469−487.
24. Siebert, F. (1995) *Methods Enzymol. 246*, 501−528.
25. Sarver, R. W. J., and Krueger, W. C. (1991) *Anal. Biochem. 199*, 61−67.
26. Fasman, G. D. (1996) *Circular Dichroism and the Conformational Analysis of Biomolecules*, Plenum, New York.
27. Woody, R. W. (1995) *Methods Enzymol. 246*, 34−70.
28. Goedert, M., Spillantini, M. G., Jakes, R., Rutherford, D., and Crowther, R. A. (1989) *Neuron 3*, 519−526.
29. Chakrabartty, A., and Baldwin, R. L. (1995) *Adv. Protein Chem. 46*, 141−176.
30. Bruch, M. D., Dhingra, M. M., and Gierasch, L. M. (1991) *Proteins: Struct., Funct., Genet. 10*, 130−139.
31. Muñoz, V., and Serrano, L. (1995) *Biochemistry 34*, 15301−15306.
32. Parry, D. A. D., and Steinert, P. M. (1999) *Q. Rev. Biophys. 32*, 99−187.
33. Wischik, C. M., Novak, M., Edwards, P. C., Klug, A., Tichelaar, W., and Crowther, R. A. (1988) *Proc. Natl. Acad. Sci. U.S.A. 85*, 4884−4888.
34. von Bergen, M., Friedhoff, P., Biernat, J., Heberle, J., Mandelkow, E. M., and Mandelkow, E. (2000) *Proc. Natl. Acad. Sci. U.S.A. 97*, 5129−5134.
35. Guijarro, J. I., Sunde, M., Jones, J. A., and Campbell, I. D. (1998) *Proc. Natl. Acad. Sci. U.S.A. 95*, 4224−4228.
36. Morozova-Roche, L. A., Zurdo, J., Spencer, A., Noppe, W., Receveur, V., Archer, D. B., Joniau, M., and Dobson, C. M. (2000) *J. Struct. Biol. 130*, 339−351.
37. Ramirez-Alvarado, M., Merkel, J. S., and Regan, L. (2000) *Proc. Natl. Acad. Sci. U.S.A. 97*, 8979−8984.
38. Eaton, W. A., and Hofrichter, J. (1990) *Adv. Protein Chem. 40*, 63−279.
39. Muñoz, V., and Serrano, L. (1994) *Nat. Struct. Biol. 1*, 399−409.
40. Richardson, J. S., and Richardson, D. C. (1988) *Science*, 1648−1652.
41. Serrano, L., Sancho, J., Hirshberg, M., and Fersht, A. R. (1992) *J. Mol. Biol. 227*, 544−559.
42. Andrew, C. D., Warwicker, J., Jones, G. R., and Doig, A. J. (2002) *Biochemistry 41*, 1897−1905.

BI025777E